Published in final edited form as:
Structure. 2013 June 4; 21(6): 939–950. doi:10.1016/j.str.2013.04.018.

A Cryptic TOG Domain with a Distinct Architecture Underlies CLASP- Dependent Bipolar Spindle Formation

Jonathan B. Leano[1], **Stephen L. Rogers**[2,3,4], and **Kevin C. Slep**[2]

[1]Dept. of Biochemistry and Biophysics, University of North Carolina, Chapel Hill, NC 27599

[2]Dept. of Biology, University of North Carolina, Chapel Hill, NC 27599

[3]Carolina Center for Genome Science, University of North Carolina, Chapel Hill, NC 27599

[4]Lineberger Comprehensive Cancer Center, University of North Carolina, Chapel Hill, NC 27599

SUMMARY

CLASP is a key regulator of microtubule (MT) dynamics and bipolar mitotic spindle structure with CLASP mutants displaying a distinctive monopolar spindle phenotype. It has been postulated that cryptic TOG domains underlie CLASP's ability regulate MT dynamics. Here, we report the crystal structure of the first cryptic TOG domain (TOG2) from human CLASP1, revealing the existence of a *bona fide* TOG array in the CLASP family. Strikingly, CLASP1 TOG2 exhibits a unique, convex architecture across the tubulin-binding surface that contrasts with the flat tubulin-binding surface of XMAP215 family TOG domains. Mutations in key, conserved TOG2 determinants abrogate the ability of CLASP mutants to rescue bipolar spindle formation in *Drosophila* cells depleted of endogenous CLASP. These findings highlight the common mechanistic use of TOG domains in XMAP215 and CLASP families to regulate MT dynamics, and suggest that differential TOG domain architecture may confer distinct functions to these critical cytoskeletal regulators.

INTRODUCTION

MTs are polymers of αβ-tubulin that facilitate cell shape change, cell migration, intracellular transport and mitotic spindle formation. The dynamic nature of the MT polymer underlies these activities. MT dynamics are tightly regulated by MT associated proteins, including the key regulator: CLASP. Human CLASP was first identified as a CLIP family associated protein (Akhmanova et al., 2001). It forms a family with two previously identified proteins: *S. cerevisiae* Stu1 (a suppressor of a β-tubulin mutation) and *Drosophila* Multiple Asters (MAST)/Orbit/Chromosome Bows, named after its mutant spindle phenotypes (Pasqualone and Huffaker, 1994; Lemos et al., 2000; Inoue et al., 2000; Fedorova et al., 1997). Homologous members have since been identified across eukaryotic species, positioning the CLASP family as conserved regulators of MT dynamics (Hannak

Correspondence: kslep@bio.unc.edu.

ACCESSION NUMBERS

The coordinates for the human CLASP1 TOG2 structure have been deposited in the Protein Data Bank under accession code 4K92.

SUPPLEMENTAL INFORMATION

Supplemental Information includes three figures, one table, and Supplemental Experimental Procedures.

and Heald, 2006; Bratman and Chang, 2007). In cells, CLASP localizes to the polymerizing MT plus end. CLASP MT plus end association is EB1-dependent, mediated through a central EB1-binding SxIP motif (Mimori-Kiyosue et al., 2005). At the MT plus end, CLASP modulates MT dynamics, promoting MT pause, stabilization and rescue during interphase (Akhmanova et al., 2001; Sousa et al., 2007; Drabek et al., 2006). During mitosis, CLASP localizes to kinetochores and promotes tubulin incorporation into fluxing kinetochore fibers (Maiato et al., 2003; Maiato et al., 2005; Cheeseman et al., 2005; Pereira et al., 2006). How CLASP differentially promotes MT pause and growth remains to be determined. Overall, CLASP is a key spatial regulator of interphase MT dynamics as well as spindle structure and dynamics, but its mechanism remains to be determined.

CLASP has a unique domain architecture. CLASP was originally annotated as having a conserved C-terminal domain used to bind CLIP-170 as well as an N-terminal TOG domain (Akhmanova et al., 2001). TOG domains are approximately 220–250 residues in length and form a pentameric array in the XMAP215 MT polymerase family (Cullen et al., 1999; Brittle and Ohkura, 2005). This TOG array works as a multivalent-tubulin binding platform, collectively modulating MT dynamics (Widlund et al., 2011; Ayaz et al., 2012). It was thus surprising that CLASP would only have a single TOG domain, since XMAP215 activity requires an array. TOG domains are composed of twelve helices, consecutively paired in six HEAT repeats (HR) (Al-Bassam et al., 2007; Slep and Vale, 2007). Intra-HEAT loops define one face of the domain, which interacts with the αβ-tubulin heterodimer (Ayaz et al., 2012). When the structure of XMAP215 family TOG domains were determined from *Drosophila* and yeast, the authors noted discontinuous determinants in two conserved central regions of the CLASP family that bore sequence similarity to TOG domain intra-HEAT loops (Slep and Vale, 2007). The authors hypothesized that these two conserved regions were cryptic TOG-like domains, whose discontinuous tubulin-binding determinants were retained, but the intervening regions had diverged, specifically the composition of the inter-HEAT loops and the lengths and surface exposed residues of the HEAT-repeat helices. The discontinuous sequence similarity with XMAP215 member TOG domains prevented standard BLAST searches from identifying CLASP's cryptic TOG domains as TOG domains and required structure-based insight. This cryptic TOG domain hypothesis suggested that CLASP, like XMAP215, might use a TOG array to regulate MT dynamics. In support of this, early work characterizing the yeast CLASP member Stu1 mapped β-tubulin binding activity to the region encompassing the first predicted cryptic TOG domain (Yin et al., 2002). Subsequent work with *Drosophila*, *S. pombe* and *Xenopus* CLASP members has implicated this region as a key mechanistic determinant in CLASP function (Slep and Vale, 2007; Al-Bassam et al., 2010; Patel et al., 2012).

Here, we present the crystal structure of the first cryptic TOG-like domain from human CLASP1. This reveals that the first cryptic TOG-like domain is a *bona fide* TOG domain. Accordingly, we designate it TOG2. Unexpectedly, CLASP1 TOG2 has a unique, bent architecture, not observed in TOG domain structures determined to date. The bent TOG architecture has concomitant implications for the conformation of αβ-tubulin complexed with CLASP and potentially underlies CLASP-dependent MT pause and rescue events. This represents the first structure of a domain from the CLASP family, establishes the presence of a TOG array in CLASP, and suggests that a potential TOG array mechanistic paradigm underlies the activities of the CLASP and XMAP215 families. We support our structural investigation with analysis of TOG2 structural determinants and their key role in bipolar mitotic spindle formation and MT polymerization.

RESULTS AND DISCUSSION

The First Cryptic TOG-Like Domain is a True TOG Domain

Secondary structure prediction of the human CLASP1 sequence predicted a dodeca-helical domain spanning residues 284–552 that bore high conservation across species (Figures 1A–B, S1). This region was subcloned, expressed, crystallized and used to seed selenomethionine-substituted crystals. A single-wavelength anomalous dispersion data set was collected to 2.0 Å resolution. The structure was phased and refined to R_{work} and R_{free} values of 18.3 and 21.0 respectively. Crystallographic statistics are presented in Table I. The asymmetric unit contains two CLASP1 molecules that are nearly identical, with a root-mean-square deviation (rmsd) of 0.5 Å across 243 Cα atoms (Figure S2A).

The architecture of the domain is an elongated, helical solenoid, composed of six HRs, largely conforming to the arrangement observed in TOG domains (Figure 1B–C)(Al-Bassam et al., 2007; Slep and Vale, 2007). The six HRs, designated HR A–F, are arranged into triads. HR A–C has a right-handed twist and abuts the HR D–F triad which is shifted laterally relative to the axes of the first triad's helices. The HR D–F triad is right-handed between HR D–E and left-handed between HR E–F. A unique feature of the CLASP1 TOG2 domain is the N-terminal helix, α2N that runs orthogonal to HR B–C helices α2B′ and α2C′. We mapped conserved residues onto the CLASP1 TOG2 structure, contouring conservation at 80% identity (green) and 80% similarity (yellow) based on a multi-species alignment (Figures S1, 1B). This revealed high conservation of solvent-exposed residues, clustered on the TOG domain surface formed by the intra-HEAT loops; these match residues in the XMAP215 family that mediate tubulin-binding (Figure 1D)(Ayaz et al., 2012). This surface also has a net positive charge (Figure 1E) that would complement the negatively charged MT surface. Additional residues, on other faces of the domain, also show a high degree of conservation. These residues either form the domain core, or are dispersed across the domain surface and are involved in inter-HR salt bridges or α2N-binding. We hypothesize that these additional conserved residues confer structural support and stability. The architecture of this conserved domain confirms our prediction that CLASP is composed of arrayed TOG domains, similar to the arrayed TOG domains of the XMAP215 family.

The Intra-HEAT Loops Carry Canonical TOG Domain Tubulin-Binding Determinants

The conserved surface-exposed intra-HEAT loop residues share similarity to characterized tubulin-binding determinants from XMAP215 family TOG domains, identified through mutagenesis and structural analysis (Al-Bassam et al., 2007; Slep and Vale, 2007). Particular insight comes from the recent low-resolution structure of the *S. cerevisiae* XMAP215 member Stu2 TOG1 domain in complex with αβ-tubulin (Ayaz et al., 2012). This structure confirmed the TOG intra-HEAT loops as prime tubulin-binding determinants. Stu2 TOG1 HR A–D engage β-tubulin while HR E–F engage α-tubulin. Many of the tubulin-binding determinants identified in these XMAP215 family studies are conserved in CLASP1 TOG2: a conserved, solvent exposed tryptophan in the HR A loop (W338, Figure 1F), a leucine residue in the HR B loop (L380, Figure 1F), a lysine residue in the HR C loop (K423, Figure 1G), and basic residues in the HR D loop (K456 and R462, Figure 1H). The role of these residues in tubulin-binding is supported by mutagenesis conducted in the *S. pombe* CLASP family member, Cls1p (Al-Bassam et al., 2010). In this study, a construct comprising Cls1p TOG1 and TOG2 was capable of binding and shifting αβ-tubulin over gel filtration, indicative of Cls1p-αβ-tubulin complex formation. When mutations in the now identified TOG2 conserved HR A and C loops were introduced, the ability of this Cls1p construct to shift αβ-tubulin was ablated. Likewise, these same mutations prevented Cls1p from stabilizing MTs *in vivo* (Al-Bassam et al., 2010). The structure and mutational studies

support the hypothesis that CLASP TOG2 interacts directly with tubulin in a mode generally similar to XMAP215 family TOG domains.

The CLASP1 TOG2 Structure Adopts a Unique, Bent Conformation that Contrasts with XMAP215 Family TOG Domains

To compare CLASP1 TOG2 to previously determined TOG domain structures, we structurally aligned CLASP1 TOG2 to Stu2 TOG1 using the Dali server (Hasegawa and Holm, 2009). The TOG domains aligned poorly overall, with an rmsd equal to 3.4 Å over 193 Cα residues (13% identity, Figure 2A). Relative to the straight tubulin-binding surface of Stu2 TOG1, this alignment revealed a surprisingly dramatic 30° shift between the predicted tubulin-binding surface of CLASP1 TOG2's first and second HR triads (Figure 2B–C, red arrow). To examine this architectural difference in more detail, we structurally aligned the first HR triad from CLASP1 TOG2 and Stu2 TOG1 and examined how this positioned the respective second HR triad of each domain. The N-terminal HR Triads, (HR A–C), again aligned poorly with an rmsd equal to 3.0 Å across 102 Cα atoms (15% identity) (Figure 2D). While the CLASP1 TOG2 intra-HEAT A and B loops align well to the Stu2 TOG1 tubulin-binding determinants, HR C is shifted towards the tubulin-binding surface as well as towards the second HR triad. In contrast to the Stu2 TOG1 HR C anti-parallel helices, the CLASP1 TOG2 HR C helices are angled relative to one another due the absence of bulky, buried hydrophobic side chains at the α2C′ N-terminal region. This effectively compresses the α2C′ N-terminal region against a2C, shifting the intra-HEAT loop towards the tubulin-binding surface and rotating the α2C′ C-terminal region outward (Figure 2E, red arrows). The unique CLASP1 TOG2 α2N N-terminal helix is likely to promote this change in HR C positioning, as it inserts two conserved phenylalanine residues (F302 and F306) between HR B and HR C (Figure 2F). The differential conformation in HR C causes the second HR triad to undergo an *en bloc* rotation away from the tubulin-binding plane established by the first HR triad, effectively displacing HR F 14 Å relative to the position of HR F in Stu2 TOG1 (Figure 2D, red arrow). When we structurally aligned the C-terminal HR Triads (HR D–F) of Stu2 TOG1 and CLASP TOG2, we were surprised to find that these triads aligned quite well, with an rmsd equal to 1.9 Å across 89 Cα atoms (10% identity) (Figure 2G). The highest degree of structural similarity in the second HR triad occurs at the intra-HEAT loops, used by Stu2 TOG1 to engage tubulin. Thus, unique determinant in CLASP1 TOG2 HR C and the α2N helix impart a bent architecture to the TOG domain. On either side of this bend-point, the CLASP TOG2 intra-HEAT loops bear structural similarity to the tubulin-binding determinants of Stu2 TOG1. Both CLASP1 TOG2 protomers in the asymmetric unit have the same bent structure with relatively low B-factors at the domain's bend site (Figure S2A–B). Crystal packing interactions are limited to the domain's flanking HRs, suggesting that the bent architecture is not due to crystal packing (Figure S2C–D). CLASP TOG2's bent architecture likely effects its interaction with αβ-tubulin and is probably a unique mechanistic determinant of CLASP-mediated MT regulation.

The CLASP1 TOG2-Tubulin Interaction is Predicted to be Dramatically Different from XMAP215 Family TOG-Tubulin Interactions

To gain insight into how CLASP1 TOG2 might interact with tubulin, we compared the structure of CLASP1 TOG2 to Stu2 TOG1 in complex with αβ-tubulin (Ayaz et al., 2012). In the Stu2 TOG1-αβ-tubulin structure, Stu2 forms extensive contacts with both β-tubulin and α-tubulin (Figure 3A). Stu2 TOG1 binds a curved tubulin conformation, predicted to mimic the structure of αβ-tubulin in solution. This contrasts with the straight conformation of tubulin determined from zinc-induced tubulin sheets, predicted to represent the structure of tubulin in the MT lattice (Nogales et al., 1998; Löwe et al., 2001). When β-tubulin from the straight tubulin structure is aligned to β-tubulin in the Stu2 TOG1-αβ-tubulin structure, α-tubulin does not engage Stu2 TOG1 HR E–F (Figure 3B).

We docked the CLASP1 TOG2 structure onto the Stu2 TOG1-αβ-tubulin complex, aligning the first HR triad of each TOG domain (as was done in Figure 2D) since this region contains the HR A tryptophan, a well-characterized TOG domain tubulin-binding determinant. While this enabled the first HR triad to engage β-tubulin effectively, the second HR triad was dramatically angled away from the curved αβ-tubulin structure (Figure 3C, red arrow). This gap was exacerbated if CLASP1 TOG2 was structurally aligned to the straight αβ-tubulin structure (Figure 3D). This was surprising since the CLASP1 TOG2 and Stu2 TOG1 second HR triads structurally align and contain similar predicted α-tubulin-binding determinants (Figure 2G). If the CLASP1 TOG2 second HR triad is to engage α-tubulin, a dramatic rearrangement in the TOG domain and/or αβ-tubulin will be required. It is of note that 1) the stabilizing α2N helix does not extend past the first HR triad to the second triad, suggesting that the two triads may undergo relative *en bloc* movement and 2) the bend between the first and second HR triad is positioned at the αβ-tubulin hinge region that changes between the straight and curved tubulin conformations. Perhaps CLASP binds an even more highly curved αβ-tubulin conformation, allowing it to stabilize the curved protofilaments observed during MT depolymerization, preventing further depolymerization. Stabilizing a curved MT plus end conformation would also inhibit polymerization since lateral tubulin contacts would be disrupted. This may underlie CLASP's ability to promote MT pause. In contrast, an inter-TOG2 structural transition to a straighter conformation may underlie the CLASP-dependent MT polymerization activity observed in mitosis.

TOG2 is Required for CLASP-Mediated Bipolar Spindle Formation

To probe the role of TOG2 and its unique structural determinants in CLASP function, we performed rescue assays in *Drosophila* S2 cells. The single *Drosophila* CLASP member, MAST/Orbit, regulates interphase MT dynamics as well as mitotic spindle structure and dynamics (Sousa et al., 2007; Lemos et al., 2000; Maiato et al., 2002; Maiato et al., 2005). Here, we concentrated our analysis on mitotic spindle structure. We treated S2 cells with control dsRNA and scored mitotic spindle structure (Figure 4A–B, Table S1). 76% of cells formed normal bipolar biastral spindles, while 10% formed bipolar monoastral spindles and 14% formed monopolar monoastral spindles. In contrast, RNAi-mediated MAST depletion produced the established monopolar monoastral spindle structure with "orbiting" "chromosome bows" (Figure 4A–B; we confirmed MAST depletion via western blot analysis; Figure 4C). 72% of cells had monopolar monoastral spindles, 14% had bipolar monoastral spindles, and only 14% had normal bipolar biastral spindles. eGFP control transfections did not alter either the wild-type or MAST RNAi distributions. This monopolar phenotype could be substantially but not completely rescued by FL MAST-Myc, decreasing the monopolar monoastral spindle index to 46% and increasing the bipolar biastral index to 42%. This failure to fully rescue spindle structure is likely due to a dominant effect of overexpression, as cells treated with control dsRNA and transfected with FL MAST-Myc had a monopolar monoastral index increased to 44%. Similar effects have been noted with the *Xenopus* member Xorbit (Patel et al., 2012). The MT stabilizing agent taxol also increases the monopolar monoastral spindle index, suggesting that MAST overexpression may hyper-stabilize MTs, causing monopolar spindle formation (Maiato et al., 2002).

This provided us with an assay to assess the ability of different MAST mutants to maintain spindle architecture when endogenous MAST was depleted. We examined the role of both its common and unique TOG determinants in MAST function. We first examined a mutant completely lacking TOG2. The ΔTOG2 construct failed to rescue spindle structure relative to the eGFP control, suggesting that MAST activity requires TOG2 (Figure 5A–B). We next examined whether a residue known to make a critical tubulin contact in other TOG domains was important for MAST function. To do so, we mutated the conserved, surface exposed HR A loop tryptophan to glutamate, a mutation known to disrupt tubulin binding activity in

XMAP215 family TOG domains (Figure 5C)(Slep and Vale, 2007). MAST W334E failed to rescue bipolar biastral spindle structure, and yielded spindle distributions on par with the ΔTOG2 construct, indicating that this key residue used in XMAP215 TOG domains to bind tubulin and promote polymerization is similarly required in MAST TOG2 to promote bipolar spindle formation (Figure 5A–B). We next individually mutated conserved basic residues in the second HR triad to glutamate: R460E in HR D, and R502E in HR E. Both R460E and R502E failed to rescue bipolar biastral spindle structure. Collectively, our data indicate that TOG2 tubulin-binding determinants in both the first and second HR triad are utilized in CLASP-dependent bipolar spindle formation. Bacterially expressed TOG2 constructs containing these mutations were purified and analyzed using circular dichroism. All constructs behaved like wild type TOG2 and produced similar CD spectra, indicative of a folded, α-helical domain (Figure 5D–G).

We next explored the role of the α2N helix, which is a unique feature of TOG2 that is not present in other TOG domain structures determined to date. The α2N helix engages HR B and C, using two conserved phenylalanine residues: F302 and F306 (F298 and F302 in MAST respectively)(Figure 2F), and may serve to stabilize and/or promote the bent TOG2 architecture. To assess whether this helix is important for MAST function, we systematically mutated each conserved phenylalanine, individually or in pairs, to either alanine or glutamate to potentially disengage it from the TOG domain. The individual phenylalanine to alanine mutations did not alter the mitotic spindle index from levels observed with FL MAST; however, the double F298A/F302A mutant as well as the individual or paired phenylalanine to glutamate mutations failed to rescue spindle structure (Figure 5A–B). Bacterially expressed MAST TOG2 constructs containing the F298E or F302E mutation proved insoluble, strongly suggesting that the α2N helix plays a key role in TOG2 domain structure and stability.

TOG2 Promotes Microtubule Lattice Association *in Vivo*

While CLASP localizes to growing MT plus ends, overexpression has been shown to result in MT lattice binding (Sousa *et al.*, 2007). We analyzed MAST truncation constructs and found a minimal construct, TOG1-2-linker, that binds the MT lattice when overexpressed (Figure 6A–B). The TOG1-2-linker construct contains the EB1-binding SxIP motif and also localizes to MT plus ends. We systematically introduced the same TOG2 point mutations that we tested in our bipolar spindle rescue assay and found that all three mutations: W334E, R460E, and R502E, individually reduced the relative amount of MAST1-2-linker on the microtubule lattice, but retained MT plus end association, likely mediated through EB1 binding to the SxIP motif. This indicates that TOG2 tubulin-binding determinants are used for MT lattice binding and further supports a direct TOG2-tubulin interaction. Because this interaction occurs along the length of the microtubule, this indicates that TOG2 can bind the straight αβ-tubulin conformation, suggesting that a conformational change within TOG2 may occur upon MT lattice binding.

TOG2 Increases Microtubule Polymerization Rates *in Vitro*

Given that CLASP promotes MT polymerization in mitosis, we next assayed if MAST TOG2 could promote microtubule polymerization *in vitro*. We performed a 90° light scattering assay to measure bulk microtubule polymerization over time in the presence of wild type or mutant MAST TOG2 constructs (Figure 7A). Tubulin alone began to polymerize after an ~400 second lag time. In contrast, the addition of TOG2 dramatically decreased the lag time to ~50 seconds and promoted rapid MT polymerization. No scattering was evident with the MAST TOG2 control. The ability of MAST TOG2 to enhance MT polymerization kinetics was diminished by point mutations in HR D (R460E) and HR E (R502E) and nearly abrogated with the W334E HR A mutation. Microscopy-based analysis

of the MT polymerization reaction at fixed times showed little MT polymerization for tubulin alone at 200 and 500 seconds, while the reaction conducted in the presence of MAST TOG2 showed the clear presence of MTs (Figure 7B). Larger CLASP constructs containing TOG2 have been shown to promote MT polymerization *in vitro* (Slep and Vale, 2007; Patel et al., 2012), but our findings distinctly ascribe MT polymerization activity to TOG2 and pinpoint key residues that underlie both this activity as well as bipolar mitotic spindle formation.

Our results confirm the prediction that CLASP carries a TOG array (Slep and Vale, 2007; Slep, 2009). However, in this TOG array, TOG2 has a distinct domain architecture not observed in other TOG domains: it is bent and has a unique N-terminal helix that runs along its side, structural features that suggest distinctive interactions with tubulin. While the bent TOG architecture may explain CLASP-induced microtubule pause, we note that our model represents only a single energy state. Whether CLASP TOG2 can sample different conformational states that underlie its differential activities: promoting microtubule pause during interphase, versus microtubule polymerization during mitosis, is an interesting question awaiting further studies. Our findings highlight a common TOG domain-mediated mechanism for the XMAP215 and CLASP families. It will be exciting to probe how CLASP's unique TOG domain interacts with tubulin and whether the flanking TOG domains: TOG1 and TOG3 also adopt unique conformations and how these domains work collectively to regulate MT dynamics in interphase and mitosis.

EXPERIMENTAL PROCEDURES

Cloning, Expression, and Protein Purification

Human CLASP1 TOG2 (residues 284–552) was subcloned into pET28 (Novagen). Protein was expressed in BL21 DE3 (pLysS) *E. coli*. Selenomethionine-substituted CLASP1 TOG2 was produced in B834 *E. coli* as described (Leahy et al., 1994). Native and selenomethionine-substituted CLASP1 TOG2 constructs were purified using Ni^{2+}-NTA (Qiagen) chromatography, digested with bovine α-thrombin and filtered over benzamadine sepharose (GE Healthcare) followed by cation exchange chromatography. *Drosophila* MAST TOG1 (residues 6–230) was cloned into pET28 and expressed and purified similar to CLASP1 TOG2 except anion exchange replaced cation exchange.

Crystallization

CLASP1 TOG2 was crystallized via hanging drop: 2 μl of 10 mg/ml protein plus 2 μl of a 1 ml well solution containing 22% PEG 3350 and 200 mM sodium citrate pH 8.25, 20° C. Crystals were frozen in Paratone-N. Native crystals were used to seed selenomethionine-substituted crystals.

Data Collection, Structure Determination, and Refinement

A selenium SAD peak data set was collected on a single crystal at the Advanced Photon Source 22-ID beamline at 100 K. Data were processed using HKL2000 (Otwinowski and Minor, 1997). Phases were determined using PHENIX (Adams et al., 2010) AutoSol. The CLASP1 TOG2 construct contains two endogenous methionines as well as a third N-terminal methionine introduced as a cloning artifact. Four selenium sites were found in the heavy atom search, correlating with two molecules in the asymmetric unit (47.5% solvent content), with a figure of merit equal to 0.43. An initial model was built using AutoBuild (PHENIX) that placed 476 residues and yielded an R_{free} of 0.27. Reiterative buildings in Coot (Emsley et al., 2010) followed by refinement runs using phenix.refine (PHENIX) were performed using real space, simulated annealing refinement protocols (temperatures: 5000 K start, 300 K final; 50 steps) and individual B-factor refinement, using experimental phase

restraints against a MLHL target. Once the R_{free} reached 0.24, individual B-factor and TLS refinement was performed using experimental phase restrains against a MLHL target. The final refinement run produced a figure of merit equal to 0.85 and an R_{free} value of 0.21. The final model includes residues 296–538 for protomers A and B and 385 water molecules. Figures were generated using PyMol (Schrödinger, LLC) and APBS (Baker et al., 2001).

Drosophila S2 Cell Expression Plasmids

Full-length MAST/Orbit cDNA (residues 1–1491) was sub-cloned into a modified pMT/V5-His A vector (Invitrogen), engineering a C-terminal myc tag. The vector drove eGFP expression off a separate promoter to mark transfected cells. MAST TOG1-2-linker (residues 1–830) was subcloned using the Gateway TopoD pEntr system (Invitrogen) into a destination vector with an N-terminal GFP tag under a pMT-inducible promoter (Invitrogen). MAST/Orbit mutant constructs were generated using the Quikchange protocol (Stratagene) and confirmed by DNA sequencing.

Cell Culture and Transfection

Drosophila S2 cells were cultured and treated with dsRNA as previously described (Rogers and Rogers, 2008). MAST constructs were transfected into *Drosophila* S2 cells using the Amaxa Nucleofector Kit II (Lonza) as described by the manufacturer's protocol. 2 μg of plasmid DNA was used for each transfection. Construct expression off the pMT promoter was induced using 500 μM copper sulfate, at which point RNAi-mediated depletion of endogenous MAST was initiated. MAST TOG1-2-linker overexpression was assayed in the absence of RNAi treatment, and cells were induce for 16 hours before imaging.

Immunofluorescence Microscopy and Mitotic Spindle Classification

S2 cell fixation protocols were adapted from previously descried methods (Rogers and Rogers, 2008). Cells transfected with full length MAST constructs were plated on concanavalin A-coated coverslips for 1.5–3.0 hours and fixed with 10% paraformaldehyde in BRB80 (80mM PIPES pH 6.8, 1mM $MgCl_2$, and 1mM EGTA) for 10 minutes. Phosphate buffered saline-Triton 0.1% (PBST) was used to permeabilize the cells and antibodies were diluted in PBST supplemented with 5% normal goat serum (Sigma). Antibodies used for immunofluorescence included mouse anti-tubulin (DM1α;1:1000) (Sigma), rabbit anti-DPLP (1:3000) (Rogers et al., 2009), and DAPI (300 nM) (Invitrogen). Primary antibodies were detected using Cy3-α-mouse (1:200) and Cy5-α-rabbit (1:1000)(Jackson ImmunoResearch Laboratories) conjugated secondary antibodies. Cells were mounted in a 10% PBS, 90% glycerol, 4% N-propyl gallate solution. Images were acquired using an Eclipse Ti microscope with a 100x oil NA-1.45 objective, driven by NIS Elements software (Nikon). Images were processed using Photoshop CS5 (Adobe Systems, Inc.) and ImageJ (NIH). Spindles were classified as bipolar biastral, bipolar monoastral, or monopolar monoastral. Each MAST construct was scored in three independent experiments with a minimum of 50 spindles scored in each experiment. P-values were calculated using two-way ANOVAs. Cells transfected with MAST TOG1-2-linker constructs were treated as above, except that after plating, cells were washed briefly in BRB80 and fixed with −20 °C methanol for 10 minutes. MAST localization was scored for MT lattice binding and MT plus end binding.

Supplementary Material

Refer to Web version on PubMed Central for supplementary material.

Acknowledgments

We thank Mark Peifer for detailed comments and Ashutosh Tripathy for technical assistance. This work is supported by March of Dimes grant FY11-434 (to K.C.S.), National Institutes of Health grants R01GM094415 (to K.C.S.), R01GM081645 (to S.L.R.), and T32GM008570 (to the Program in Molecular and Cellular Biophysics), and a National Science Foundation Graduate Research Fellowship (to J.B.L.).

References

Adams PD, Afonine PV, Bunkoczi G, Chen VB, Davis IW, Echols N, Headd JJ, Hung LW, Kapral GJ, Grosse-Kunstleve RW, et al. PHENIX: a comprehensive Python-based system for macromolecular structure solution. Acta Crystallogr D Biol Crystallogr. 2010; 66:213–221. [PubMed: 20124702]

Akhmanova A, Hoogenraad CC, Drabek K, Stepanova T, Dortland B, Verkerk T, Vermeulen W, Burgering BM, De Zeeuw CI, Grosveld F, et al. Clasps are CLIP-115 and -170 associating proteins involved in the regional regulation of microtubule dynamics in motile fibroblasts. Cell. 2001; 104:923–935. [PubMed: 11290329]

Al-Bassam J, Kim H, Brouhard G, van Oijen A, Harrison SC, Chang F. CLASP promotes microtubule rescue by recruiting tubulin dimers to the microtubule. Dev Cell. 2010; 19:245–258. [PubMed: 20708587]

Al-Bassam J, Larsen NA, Hyman AA, Harrison SC. Crystal structure of a TOG domain: conserved features of XMAP215/Dis1-family TOG domains and implications for tubulin binding. Structure. 2007; 15:355–362. [PubMed: 17355870]

Ayaz P, Ye X, Huddleston P, Brautigam CA, Rice LM. A TOG:alphabeta-tubulin complex structure reveals conformation-based mechanisms for a microtubule polymerase. Science. 2012; 337:857–860. [PubMed: 22904013]

Baker NA, Sept D, Joseph S, Holst MJ, McCammon JA. Electrostatics of nanosystems: application to microtubules and the ribosome. Proc Natl Acad Sci U S A. 2001; 98:10037–10041. [PubMed: 11517324]

Bratman SV, Chang F. Stabilization of overlapping microtubules by fission yeast CLASP. Dev Cell. 2007; 13:812–827. [PubMed: 18061564]

Brittle AL, Ohkura H. Mini spindles, the XMAP215 homologue, suppresses pausing of interphase microtubules in Drosophila. EMBO J. 2005; 24:1387–1396. [PubMed: 15775959]

Cheeseman IM, MacLeod I, Yates JR 3rd, Oegema K, Desai A. The CENP-F-like proteins HCP-1 and HCP-2 target CLASP to kinetochores to mediate chromosome segregation. Curr Biol. 2005; 15:771–777. [PubMed: 15854912]

Cullen CF, Deak P, Glover DM, Ohkura H. mini spindles: A gene encoding a conserved microtubule-associated protein required for the integrity of the mitotic spindle in Drosophila. J Cell Biol. 1999; 146:1005–1018. [PubMed: 10477755]

Drabek K, van Ham M, Stepanova T, Draegestein K, van Horssen R, Sayas CL, Akhmanova A, Ten Hagen T, Smits R, Fodde R, et al. Role of CLASP2 in microtubule stabilization and the regulation of persistent motility. Curr Biol. 2006; 16:2259–2264. [PubMed: 17113391]

Emsley P, Lohkamp B, Scott WG, Cowtan K. Features and development of Coot. Acta Crystallogr D Biol Crystallogr. 2010; 66:486–501. [PubMed: 20383002]

Fedorova SA, Chubykin VL, Gucachenko AM, Omel'ianchuk LV. Mutation chromosome bows (chb-v40), inducing the abnormal chromosome spindle in Drosophila melanogaster. Genetika. 1997; 33:1502–1509. [PubMed: 9480214]

Hannak E, Heald R. Xorbit/CLASP links dynamic microtubules to chromosomes in the Xenopus meiotic spindle. J Cell Biol. 2006; 172:19–25. [PubMed: 16390996]

Hasegawa H, Holm L. Advances and pitfalls of protein structural alignment. Curr Opin Struct Biol. 2009; 19:341–348. [PubMed: 19481444]

Inoue YH, do Carmo Avides M, Shiraki M, Deak P, Yamaguchi M, Nishimoto Y, Matsukage A, Glover DM. Orbit, a novel microtubule-associated protein essential for mitosis in Drosophila melanogaster. J Cell Biol. 2000; 149:153–166. [PubMed: 10747094]

Leahy DJ, Erickson HP, Aukhil I, Joshi P, Hendrickson WA. Crystallization of a fragment of human fibronectin: introduction of methionine by site-directed mutagenesis to allow phasing via selenomethionine. Proteins. 1994; 19:48–54. [PubMed: 8066086]

Lemos CL, Sampaio P, Maiato H, Costa M, Omel'yanchuk LV, Liberal V, Sunkel CE. Mast, a conserved microtubule-associated protein required for bipolar mitotic spindle organization. EMBO J. 2000; 19:3668–3682. [PubMed: 10899121]

Lowe J, Li H, Downing KH, Nogales E. Refined structure of alpha beta-tubulin at 3.5 A resolution. J Mol Biol. 2001; 313:1045–1057. [PubMed: 11700061]

Maiato H, Fairley EA, Rieder CL, Swedlow JR, Sunkel CE, Earnshaw WC. Human CLASP1 is an outer kinetochore component that regulates spindle microtubule dynamics. Cell. 2003; 113:891–904. [PubMed: 12837247]

Maiato H, Khodjakov A, Rieder CL. Drosophila CLASP is required for the incorporation of microtubule subunits into fluxing kinetochore fibres. Nat Cell Biol. 2005; 7:42–47. [PubMed: 15592460]

Maiato H, Sampaio P, Lemos CL, Findlay J, Carmena M, Earnshaw WC, Sunkel CE. MAST/Orbit has a role in microtubule-kinetochore attachment and is essential for chromosome alignment and maintenance of spindle bipolarity. J Cell Biol. 2002; 157:749–760. [PubMed: 12034769]

Mimori-Kiyosue Y, Grigoriev I, Lansbergen G, Sasaki H, Matsui C, Severin F, Galjart N, Grosveld F, Vorobjev I, Tsukita S, et al. CLASP1 and CLASP2 bind to EB1 and regulate microtubule plus-end dynamics at the cell cortex. J Cell Biol. 2005; 168:141–153. [PubMed: 15631994]

Nogales E, Wolf SG, Downing KH. Structure of the alpha beta tubulin dimer by electron crystallography. Nature. 1998; 391:199–203. [PubMed: 9428769]

Otwinowski Z, Minor W. Processing of x-ray diffraction data collected in oscillation mode. Methods Enzymol. 1997; 276:307–326.

Pasqualone D, Huffaker TC. STU1, a suppressor of a beta-tubulin mutation, encodes a novel and essential component of the yeast mitotic spindle. J Cell Biol. 1994; 127:1973–1984. [PubMed: 7806575]

Patel K, Nogales E, Heald R. Multiple domains of human CLASP contribute to microtubule dynamics and organization in vitro and in Xenopus egg extracts. Cytoskeleton (Hoboken). 2012; 69:155–165. [PubMed: 22278908]

Pereira AL, Pereira AJ, Maia AR, Drabek K, Sayas CL, Hergert PJ, Lince-Faria M, Matos I, Duque C, Stepanova T, et al. Mammalian CLASP1 and CLASP2 cooperate to ensure mitotic fidelity by regulating spindle and kinetochore function. Mol Biol Cell. 2006; 17:4526–4542. [PubMed: 16914514]

Rogers GC, Rusan NM, Roberts DM, Peifer M, Rogers SL. The SCF Slimb ubiquitin ligase regulates Plk4/Sak levels to block centriole reduplication. J Cell Biol. 2009; 184:225–239. [PubMed: 19171756]

Rogers SL, Rogers GC. Culture of Drosophila S2 cells and their use for RNAi-mediated loss-of-function studies and immunofluorescence microscopy. Nat Protoc. 2008; 3:606–611. [PubMed: 18388942]

Slep KC. The role of TOG domains in microtubule plus end dynamics. Biochem Soc Trans. 2009; 37:1002–1006. [PubMed: 19754440]

Slep KC, Vale RD. Structural basis of microtubule plus end tracking by XMAP215, CLIP-170, and EB1. Mol Cell. 2007; 27:976–991. [PubMed: 17889670]

Sousa A, Reis R, Sampaio P, Sunkel CE. The Drosophila CLASP homologue, Mast/Orbit regulates the dynamic behaviour of interphase microtubules by promoting the pause state. Cell Motil Cytoskeleton. 2007; 64:605–620. [PubMed: 17487886]

Widlund PO, Stear JH, Pozniakovsky A, Zanic M, Reber S, Brouhard GJ, Hyman AA, Howard J. XMAP215 polymerase activity is built by combining multiple tubulin-binding TOG domains and a basic lattice-binding region. Proc Natl Acad Sci U S A. 2011; 108:2741–2746. [PubMed: 21282620]

Yin H, You L, Pasqualone D, Kopski KM, Huffaker TC. Stu1p is physically associated with beta-tubulin and is required for structural integrity of the mitotic spindle. Mol Biol Cell. 2002; 13:1881–1892. [PubMed: 12058056]

HIGHLIGHTS

- The CLASP family contains a cryptic TOG domain array
- CLASP TOG2 has a unique, bent architecture across the tubulin-binding surface
- CLASP TOG2 determinants are required for proper bipolar spindle formation

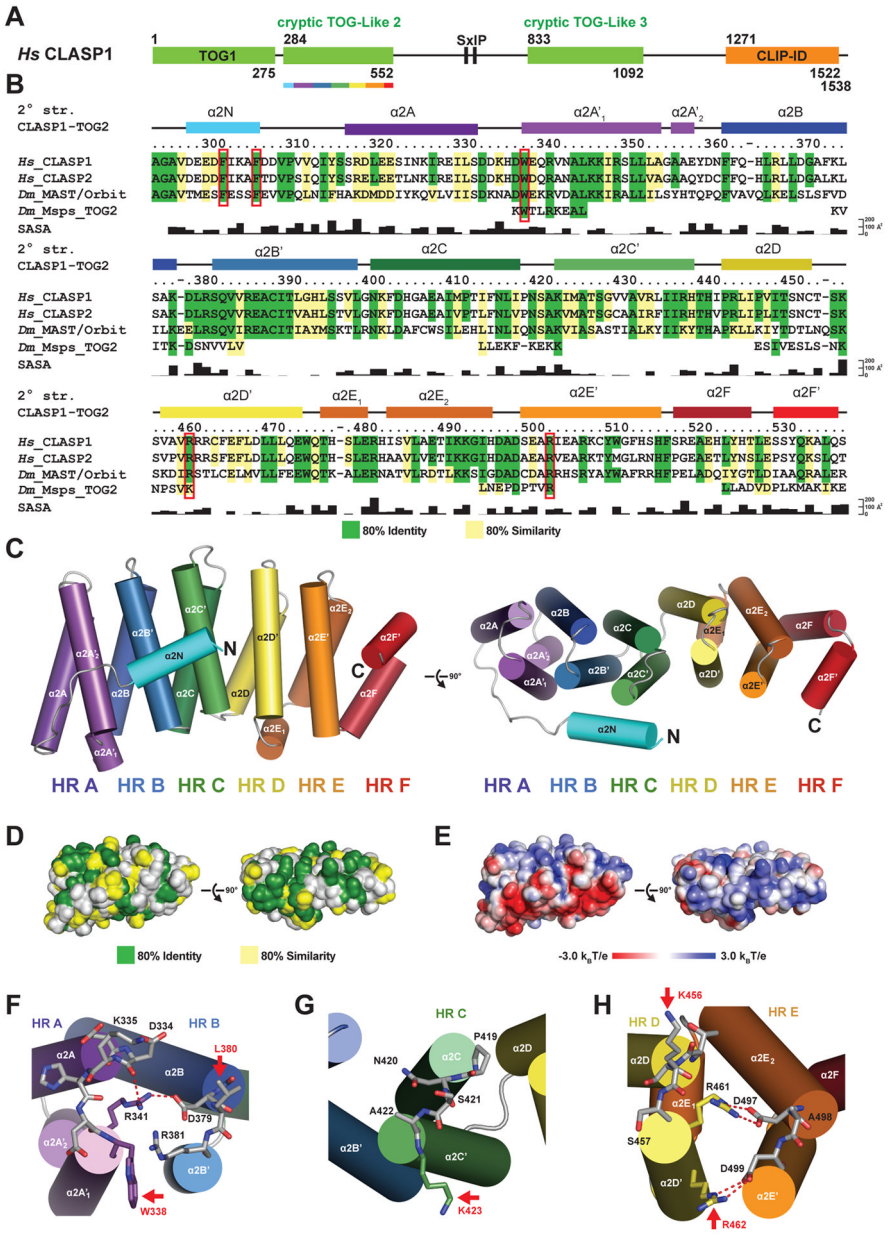

Figure 1. CLASP Contains a Conserved, Cryptic TOG Array

(A) Human CLASP1 domain architecture showing the four conserved domains: the annotated TOG1 domain, two cryptic TOG-like domains (TOG2 and TOG3), and the CLIP interaction domain (CLIP-ID). (B) Sequence alignment of human (*Hs*) CLASP1, CLASP2 and *Drosophila* (*Dm*) MAST/Orbit TOG2. Identity (green) and similarity (yellow) are contoured at 80% based on the alignment in Figure S1. Numbering corresponds to human CLASP1. *Drosophila* Msps TOG2 intra-HEAT loop sequences are aligned. MAST residues mutated for cellular studies are boxed in red. See also Figure S1. (C) Human CLASP1 TOG2 structure, composed of HR A–F. The N-terminal helix, α2N, runs orthogonal to the HRs. See also Figure S2. (D) CLASP1 TOG2 oriented as in C, shown in surface representation with conservation mapped as in B. See also Figure S2. (E) Electrostatic surface potential mapped on CLASP1 TOG2, oriented as in D. (F) Intra-HEAT loops from HR 2A and 2B. Hydrogen bonds (< 3.5 Å) shown in red. The conserved TOG domain

tubulin-binding determinant, W338, is solvent exposed. (G) The HR 2C intra-HEAT loop contains the conserved, solvent-exposed residue K423, implicated in tubulin binding (Al-Bassam et al., 2010). (H) The HR 2D intra-HEAT loop contains the conserved, solvent-exposed basic residues K456 and R462, which correspond to TOG-tubulin binding determinants in Stu2 (Ayaz et al., 2012). Residues noted shown with red arrows.

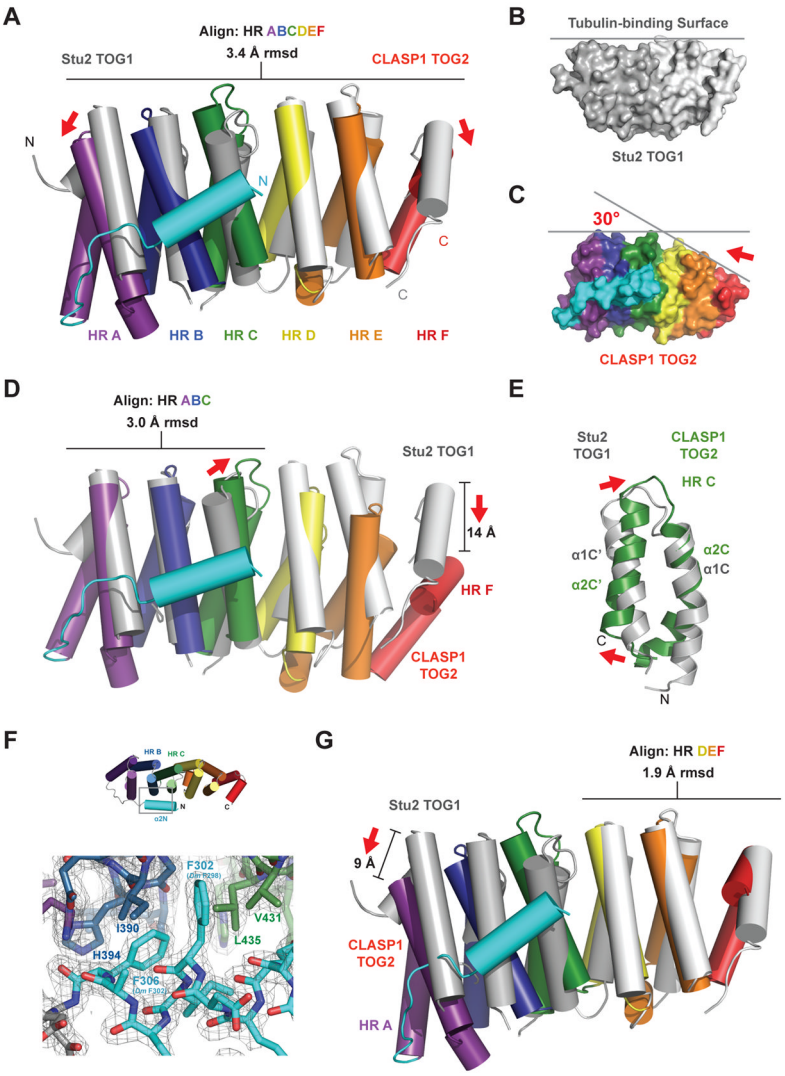

Figure 2. CLASP1 TOG2 has a Unique, Bent Structure

(A) CLASP1 TOG2 (colored as in Figure 1C) and *S.c.* XMAP215 member Stu2 TOG1 (4FFB, HR triads: HR A–C and HR D–F shown in two shades of grey) aligned over HR A–F. The alignment highlights the bent architecture of CLASP1 TOG2 (red arrows). (B, C) Surface representation of Stu2 TOG1 (B) and CLASP1 TOG2 (C) orientated as in D, showing the flat Stu2 TOG1 tubulin-binding surface versus the bent CLASP1 TOG2 surface. The intra-HEAT A–C and D–F loops form two surfaces, angled 30° relative to each other (red arrow). (D) CLASP1 TOG2 and Stu2 TOG1 as in A, aligned over HR AC. (E) CLASP1 TOG2 (green) and Stu2 TOG1 (grey) HR C aligned as in D, highlighting the structural divergence in the αC and αC′ helices (red arrows) which offsets the relative position of HR D–F. (F) Structure of CLASP1 TOG2 α2N residues F302 and F306 (MAST F298 and F302 respectively) that pack between HR B and C ($2F_o$-F_c electron density map in grey, 1.5σ). (G) CLASP1 TOG2 and Stu2 TOG1 as in A, aligned over HR D–F.

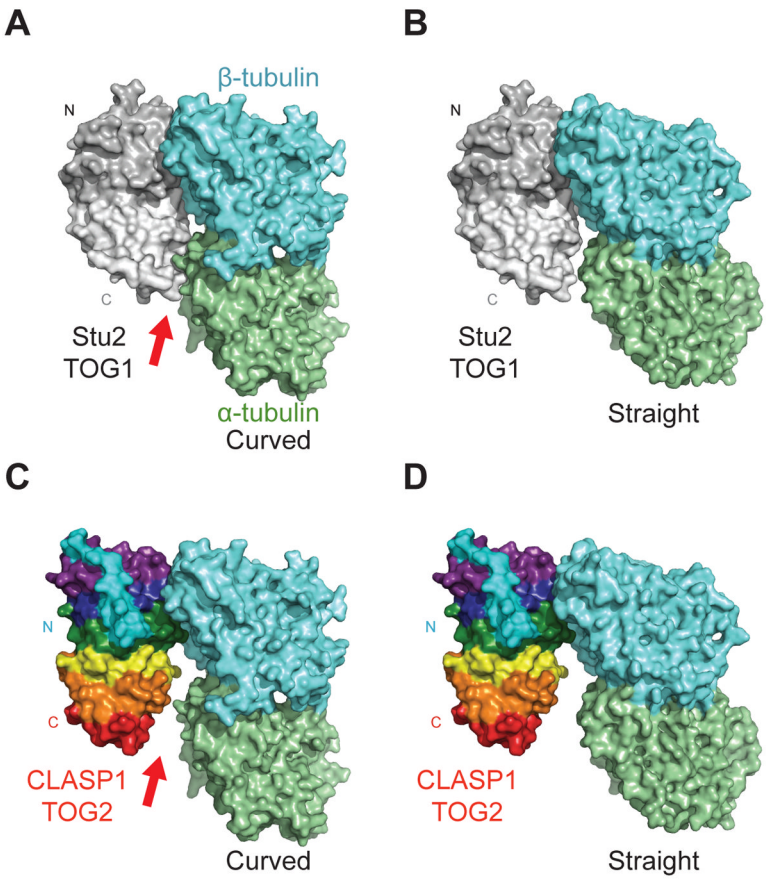

Figure 3. CLASP1 TOG2 and/or αβ-Tubulin is Likely to Undergo Conformational Change Upon Binding

(A) Structure of the Stu2 TOG1-αβ-tubulin complex (4FFB). Stu2 is colored as in Figure 2A. Stu2 TOG1 binds curved αβ-tubulin. (B) Model of Stu2 TOG1 docked onto straight (MT-like) αβ-tubulin (1JFF) by aligning β-tubulin from IJFF and 4FFB. The straight αβ-tubulin conformation creates a gap between α-tubulin and Stu2 TOG1 HR D–F. (C) CLASP1 TOG2 superimposed on the 4FFB structure after alignment across HR A–C as in Figure 2D (Stu2 not shown). While CLASP1 TOG2 HR A–C can engage β-tubulin using similar binding determinants, HR D–F is splayed 30° from α-tubulin (red arrow). (D) Model of CLASP1 TOG2 docked onto straight tubulin yields a larger gap between CLASP1 TOG2 and α-tubulin.

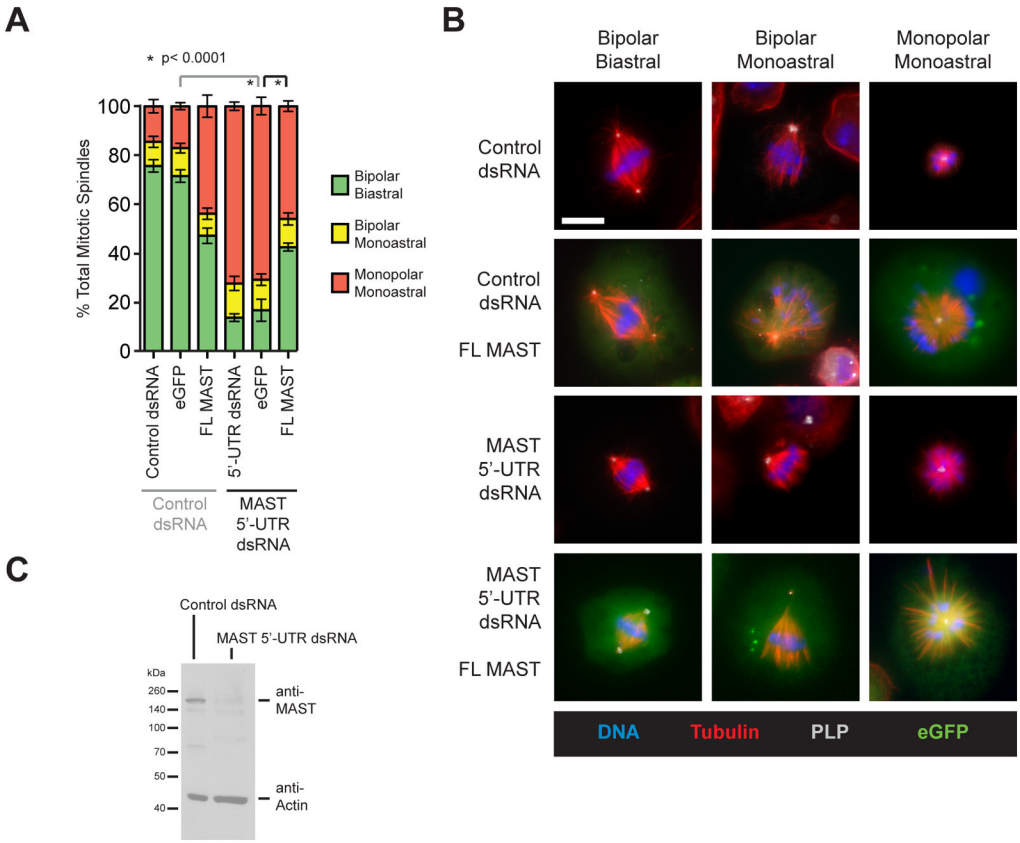

Figure 4. MAST Depletion Causes Bipolar Spindle Defects that can be Partially Rescued in *Trans*

(A) Mitotic spindle classification from *Drosophila* S2 cells treated with control or MAST 5′-UTR-directed dsRNA, transfected with the indicated MAST construct. Spindles were classified as bipolar biastral, bipolar monoastral, or monopolar monoastral. Error bars represent standard deviation. See also Table S1. (B) Representative images of spindles used to tally the distribution showed in A. Cells were stained with anti-PLP, DAPI, and DM1α to label centrosomes, DNA, and MTs respectively. Scale bar: 10 μm. See also Figure S3. (C) Western blot showing effective MAST depletion.

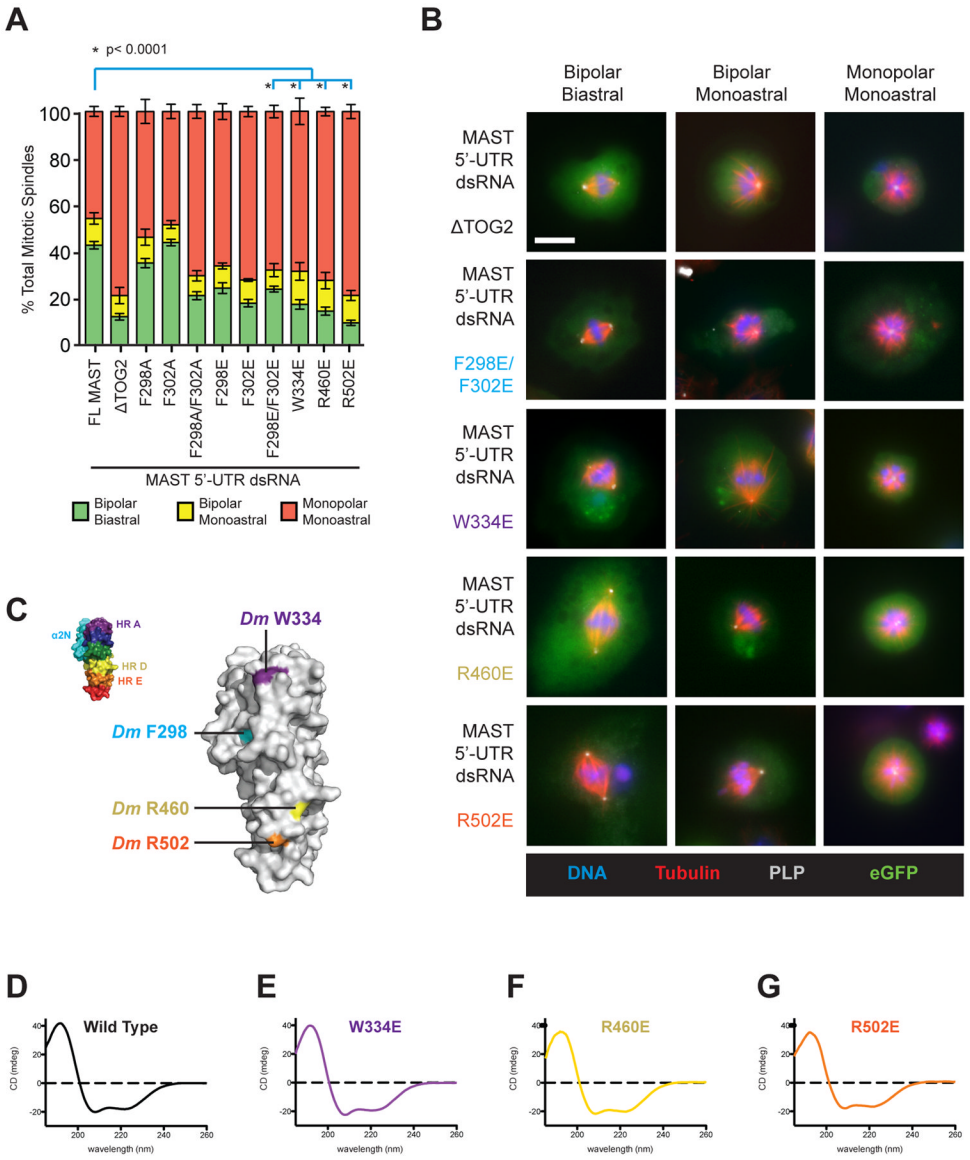

Figure 5. Point Mutations Across the TOG2 Tubulin-Binding Surface Fail to Rescue MAST-mediated Bipolar Spindle Formation

(A) Mitotic spindle classification from *Drosophila* S2 cells treated with control or MAST 5′-UTR-directed dsRNA, transfected with the indicated MAST construct. Spindles were classified as in Figure 4A. Error bars represent standard deviation. See also Table S1. (B) Representative images of spindles used to tally the distribution showed in A. Cells were stained as in Figure 4B. Scale bar: 10 μm. See also Figure S3. (C) Domain architecture of human CLASP1 TOG2 showing the location of identical, couterpart residues in *Drosophila* MAST TOG2 that were individually mutated to glutamate in α2N (*D. m.* F298), HRA (*D.m.* W338), HRD (*D.m.* R461), and HRE (*D.m.* R503). (D–G) Circular dichroism spectra of wild type MAST TOG2 (D), W334E (E), R460E (F), and R502E (G), each showing similar spectra characteristic of an α-helical protein, indicative that all mutants retained a similar folded state.

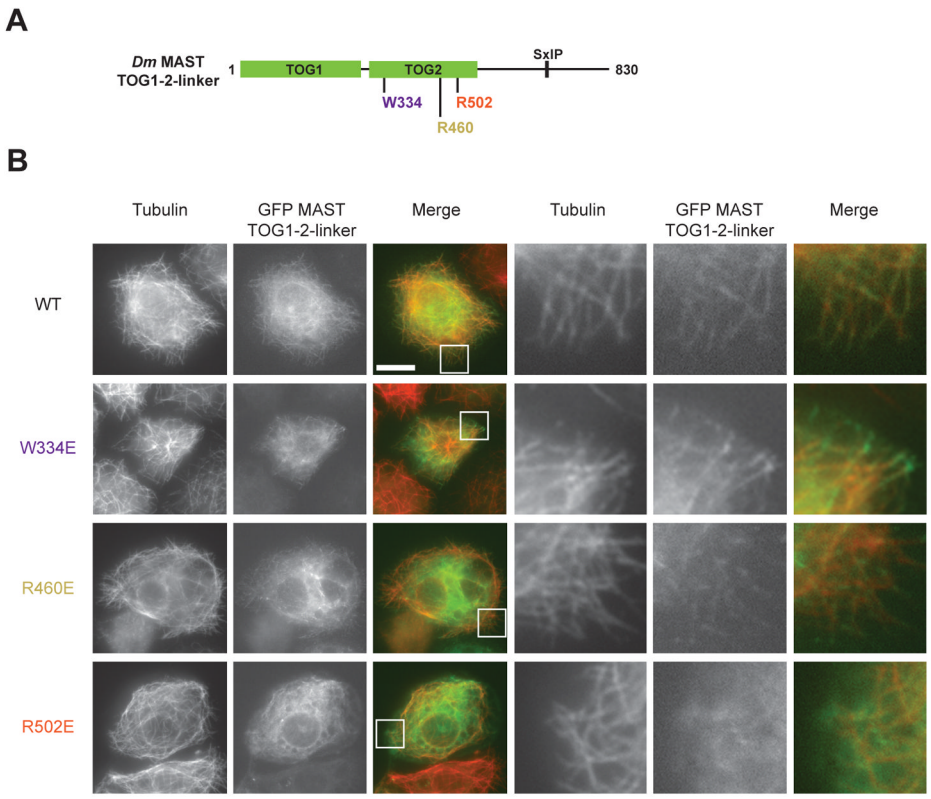

Figure 6. MAST TOG2 Determinants Mediate MT-lattice Binding

(A) Domain organization of the MAST TOG1-2-linker construct. The relative location of TOG2 domain mutations are indicated as is the linker region's EB1-binding SxIP motif. (B) *Drosophila* S2 cells transfected with the indicated GFP MAST TOG1-2-linker construct. Cells were strained with DM1α to label MTs. Merge shows GFP in green and tubulin in red and the box inset is shown in zoom view in the three panels to the right. Scale bar: 10 μm.

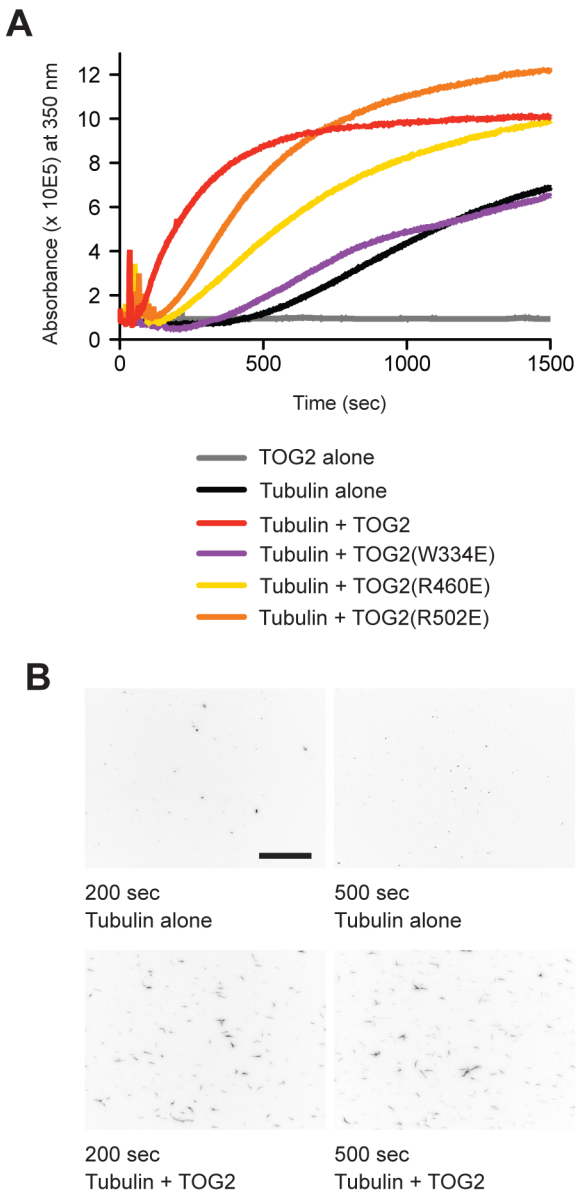

Figure 7. MAST TOG2 Promotes MT Polymerization *in Vitro*

(A) 90° light scattering curves (350 nm) performed on tubulin (15 μM) at 37° C in the presence or absence of MAST TOG2 constructs (1.4 μM) (see legend). Initial spikes in scattering within the first 100 seconds were the result of samples equilibrating to 37° C. The TOG2 alone control showed no scattering contribution over time (grey trace). (B) Images of tubulin alone and tubulin plus MAST TOG2 polymerization samples fixed and diluted at 200 and 500 second time points. MTs were stained with DM1α. Scale bar: 50 μm.

Table 1

Crystallographic Data and Refinement Statistics

Data Collection	
Wavelength (Å)	0.980377
Space group	$P2_12_12_1$
Cell dimensions: a, b, c (Å)	62.3, 66.5, 138.9
Resolution (Å)	20.0–2.00 (2.07–2.00)
# Reflections: Measured/Unique	68,739 (4,858)/10,919 (1,278)
Completeness (%)	92.3 (64.9)
Mean redundancy	6.3 (3.8)
<I/σI>	16.7 (3.9)
R_{sym} [a]	0.09 (0.278)
Refinement	
Resolution (Å)	20.0–2.00 (2.05–2.00)
R^b/R_{free} (%)[c]	18.3 (22.3)/21.0 (28.7)
# Reflections, R/R_{free}	34,474 (1,525)/1,960 (79)
Total atoms: Protein/Water	3,912/385
Stereochemical ideality (rmsd): Bonds/ Angles (Å/°)	0.014/1.15
Mean B-factors (Å^2): Overall/Protein/ Water	34.8/34.1/41.3
Ramachandran Analysis: Favored/ Allowed (%)	99.2/0.8

[a] $R_{sym} = \Sigma_h \Sigma_i |I_i(h) - \langle I(h) \rangle| / \Sigma_h \Sigma_i I_i(h)$ where $I_i(h)$ is the integrated intensity of the ith reflection with the Miller Index h and $\langle I(h) \rangle$ is the average over Friedel and symmetry equivalents.

[b] R value = $\Sigma (|F_{obs}| - k|F_{calc}|)/\Sigma |F_{obs}|$.

[c] R_{free} is calculated using a 5% subset of the data that are removed randomly from the original data and excluded from refinement.